Aerosol and Air Quality Research, 14: 1584–1592, 2014

ISSN: 1680-8584 print / 2071-1409 online
doi: 10.4209/aaqr.2013.11.0331

Numerical Simulation of Airflow Structure and Dust Emissions behind Porous Fences Used to Shelter Open Storage Piles

Chong-Fang Song[1], Lin Peng[1*], Jun-Ji Cao[2], Ling Mu[1], Hui-Ling Bai[1], Xiao-Feng Liu[1]

[1] *College of Environmental Science and Engineering, Taiyuan University of Technology, 79 Yingze West Street, Taiyuan 030024, China*
[2] *Key Laboratory of Aerosol, SKLLQG, Institute of Earth Environment, Chinese Academy of Sciences, Xi'an 710075, China*

ABSTRACT

Porous fences can reduce dust emissions from storage piles in open storage yards, but their sheltering effect depends on the airflow structure around the pile, and the shear stress distribution on each surface. In this study, static flow fields were numerically simulated using the standard *k-ε* turbulence model; the shear stress characteristics and distribution on the windward side, flat-top surface, and leeward side of a typical prismatic material stack were analyzed. The distribution of the aerodynamic structure of each surface of the storage pile was determined according to the flow field data for fences of the porosities ε = 0, 0.2, 0.3, 0.4, 0.5, and 0.6. The results indicated that at low porosities (ε = 0, 0.2) a recirculating flow appeared in the region between the fence and the pile. The shear force acted downward the windward slope, and the maximum dust emission occurred at two-thirds the height of the windward side, rather than at the top, as in unfenced conditions. Using the porous fence simulated in this study, shear stress on the windward side and the flat-top surface first decreased, then increased with increasing porosity; the lowest porosity values were 0.2 and 0.3, and the shear stress on the prismatic leeside changed little with increasing porosity. The numerical predictions indicated that a fence with porosity between 0.2 and 0.3 is optimal.

Keywords: Computational fluid dynamics (CFD); Open storage pile; Dust emission; Porous fence.

INTRODUCTION

Dust emissions from open storage piles constitute a substantial portion of atmospheric particulates, and wind-blown dust emissions cause heavy air pollution in addition to material losses. Porous fences effectively reduce dust emissions from store piles in open storage yards, but turbulence fields of airflows behind porous fences substantially influence their sheltering efficiency.

Field tests and atmospheric boundary layer wind tunnel experiments have been performed to study airflows around porous fences (Gillette, 1978; Heisler and Dewalle, 1988; Xuan and Robins, 1994); however, such research is time-consuming and expensive. In recent years, computational fluid dynamics (CFD) techniques have been effectively used to determine fluid flows and calculate the mean velocity profiles of far wakes behind solid obstacles. The flow characteristics around a two-dimensional triangular-shaped prism located behind a porous wind fence have been investigated numerically by using the RNG (Renormalization Group) k-ε turbulence model (Kim *et al.*, 1997; Lee and Lim, 2001; Lee and Kim, 1999). The relationship between the screen pressure coefficient and porosity was determined to calculate the entrapment of particles by windbreaks (Raupach *et al.*, 2001). The three-dimensional wind field structure around piles of different shapes has been simulated (White and Tsoar, 1998; Parsons *et al.*, 2004; Badr *et al.*, 2005; Torano *et al.*, 2006; Badr *et al.*, 2007). The effect of clipping on stockpile dust emission rates has been estimated using the EPA's emission factors method, and information on optimal geometric pile characteristics to limit particle emissions has been provided to industrial operators (Turpin and Harion, 2009; Yeh *et al.*, 2010; Zhang *et al.*, 2011; Cong *et al.*, 2012). A quantitative evaluation of total fugitive dust, given even wind flow around a complex yard, was performed by implementing new subroutines in standard CFX software (Diego *et al.*, 2009). The reduction effect on wind velocity was measured between adjacent fences up to a height of 0.6 m from the ground, and 0.2 was determined to be the optimal porosity value: ε = 0.2, 0.4, 0.6 (Bitog *et al.*, 2009). Of the parameters used to characterize the turbulence fields (vorticity, turbulence intensity, Reynolds stress, and turbulent kinetic energy), only turbulence intensity was observed to be directly related to fence shelter

* Corresponding author.
Tel.: +86-351-6010799, Fax: +86-351-6010192
E-mail address: plin123@eyou.com

efficiency regarding sediment transport on the surface; the magnitude of the other parameters near the surface was insignificant (Dong *et al.*, 2007; Dong *et al.*, 2010).

These previous studies provided an improved understanding of airflow structures and dust emissions behind porous fences used to shelter open storage piles. The structure of air flowing over a prismatic material stack differs between regions near the stack surface, and the principle and quantity of the resulting dust emissions depend on the aerodynamic structure of all surfaces. To date, numerical simulations of flow fields around storage piles have primarily focused on mean surface stress and wind speed (Mao *et al.*, 2013), neglecting the directionality of air velocity and stresses on various surfaces. In unfenced conditions, the air flows along the pile's surfaces in incoming air direction all the time. The presence of fences will definitely affect flow regime, particularly in the region between the fence and the pile, so airflow structure shows difference with the regions near stockpile surface. Ignoring the directionality of air speed will introduce the computation distortion caused by vector offset of the shear force in opposite direction. We thus, believe that a comprehensive analysis of complex flow structures near stockpiles behind porous wind fences is necessary to predict shear stress distributions.

This study is intended to reveal the internal relations between the sheltering effect and the shear stress distribution on each surface of the storage pile. In this study, a new judgment method of macroscopic variable remaining constant was applied to deal with infinite open space as a bounded computational domain. We presented the shear stress distribution of the windward side, flat-top surface and leeward side of the typical prismatic material stack. This approach has the advantage of providing more detailed information on the airflow fields behind porous fences. Studies including the vector fields of flow proved the placement of porous fences mainly changed the flow regime characteristics, not just reduce wind speed. We have also attempted to provide optimal fence porosity based on a deeper understanding of the shear stress distribution on each surface.

NUMERICAL SIMULATION

Wind-blown particles movement from open store piles is complicated because highly turbulent flow fields is formed by the interaction between bleed flow passing through the holes of the fences and displaced flow passing over the fences. However, field tests and atmospheric boundary layer wind tunnel experiments have difficulties in obtaining detailed information close to fences and pile, and measurements will also influence the flow fields to some extent. With the development of CFD technology, methods of numerical simulation have been used more and more widely in flow simulation, especially in simulating complex flow fields. Using this method, we can acquire the whole air flow fields behind fences, and then obtain the shear stress distribution on each surface of material stack.

Numerical simulation was divided into three steps. First, the size of the computational area was defined and macro parameters, such as airflow speed, were calculated. The computational area was determined as the domain in which the macro parameter value did not change with the calculation area size, and was meshed with the calculation domain. Second, the airflow around the pile was simulated, and the appropriate turbulence model, algorithm, and discrete format were selected. Finally, the optimal porosity was determined by calculating aerodynamic parameters on the pile surface at various fence porosities.

Governing Equations and Boundary Conditions

Turbulent shear layers, separated from the surfaces of porous fences, complicate flows over prismatic piles. The RNG k-ε turbulence model was judged to be suitable to compute the separated shear flow (Kim *et al.*, 1997). Airflow is assumed to be viscous, incompressible, isothermal, and steady (Chen *et al.*, 2012), and the governing equations used to determine the continuous flow are as follows (Rosenfeld *et al.*, 2010).

Mass conservation equation:

$$\frac{\partial u_i}{\partial x_i} = 0 \tag{1}$$

Momentum conservation equation:

$$\rho u_j \frac{\partial u_i}{\partial x_j} = -\frac{\partial p}{\partial x_i} + \frac{\partial}{\partial x_j}\left(\mu \frac{\partial u_i}{\partial x_j} - \rho \overline{u_i' u_j'} \right) + S_i \tag{2}$$

where S_i is a source term assumed to be zero at all locations except on the porous fence surface (Guo *et al.*, 2012). The ability of the porous fence to act as a wind momentum sink was accounted for by applying a porous jump condition in the standard fluid flow equation. The porous jump was modeled in two parts: a viscous loss term (I) and inertial loss term (II), shown in Eq. (3).

$$S_i = -\left(\underbrace{\frac{\mu}{\alpha}}_{\text{I}} + \underbrace{C_2 \frac{1}{2} \rho |u| u_i}_{\text{II}} \right) \tag{3}$$

where α represents the permeability of the porous medium, and C_2 is an inertial resistance coefficient expressed as

$$C_2 = \frac{1}{C^2} \frac{\left(A_p / A_f \right)^2 - 1}{t} \tag{4}$$

where A_f is the area of the holes, A_p is the total area of the fence, t is the thickness of the porous medium, and C is the coefficient changed with the Reynolds number (Re) determined by the holes' diameter and the fluid velocity flowing through the holes. When Re exceeded 4000, C is approximately equal to 0.98. In this study, because Re > 4000, the value of C was set at 0.98 in the model.

To determine $-\overline{\rho u_i' u_j'}$ in Eq. (2), equations for k and ε were supplemented. This was an incompressible airflow study, and the buoyancy term was largely neglected because of the nearly negligible impact of the temperature difference. The transport equations used were as follows:

k equation:

$$\rho u_j \frac{\partial k}{\partial x_j} = \frac{\partial}{\partial x_i}\left[\left(\mu + \frac{\mu_t}{\sigma_k}\right)\frac{\partial k}{\partial x_j}\right] + G_k - \rho\varepsilon \quad (5)$$

ε equation:

$$\rho u_j \frac{\partial \varepsilon}{\partial x_j} = \frac{\partial}{\partial x_i}\left[\left(\mu + \frac{\mu_t}{\sigma_\varepsilon}\right)\frac{\partial \varepsilon}{\partial x_j}\right] + C_{1\varepsilon}\frac{\varepsilon}{k}G_k - C_{2\varepsilon}\rho\frac{\varepsilon^2}{k} \quad (6)$$

where $-\overline{\rho u_i' u_j'} = \mu_t\left(\frac{\partial u_i}{\partial x_j} + \frac{\partial u_j}{\partial x_i}\right) - \frac{2}{3}\rho k\delta_{ij}$

In which $\mu_t = \rho C_\mu \frac{k^2}{\varepsilon}$ is the viscosity coefficient of turbulence, and G_k is the outcome of the turbulence energy generated by the averaged time velocity gradient: $G_k = -\rho\overline{u_i' u_j'}\frac{\partial u_j}{\partial x_i}$, $G_k = \mu_t S^2$, $S = \sqrt{2S_{ij}S_{ij}}$, $S_{ij} = \frac{1}{2}\left(\frac{\partial u_i}{\partial x_j} + \frac{\partial u_j}{\partial x_i}\right)$

The other parameters are listed in Table 1.

The CFD model was applied to simulate the airflow structure behind a simulated porous fence and material pile. The pile was 154 m long and 51 m wide on its lower surface, 113 m long and 10 m wide on its upper surface, and 17 m high. A vertical fence with a height of 22 m was located 17 m (the same as the height of the pile) in front of the pile. An adequately large computational domain ensures that the simulated airflow field is unrelated to the computational domain, but requires a large number of calculations. To avoid this, numerical simulations for seven models with various physical dimensions were examined and the optimal computational domain was determined to be when the shear stress on the flat-top surface ceased changing. The computational domain is shown in Fig. 1, the parameters for the seven calculation areas are shown in Table 2, and the boundary conditions are shown in Table 3.

Table 1. Input value for numerical simulation.

Parameter	Units	Symbol	Value
Atmospheric pressure	Pa	P	101325
Air temperature	K	T	293
Air density	kg/m^3	ρ	1.225
Air dynamic viscosity	N·/m^2	μ	1.79×10^{-5}
k-ε turbulence model constant		$C_{1\varepsilon}$	1.44
k-ε turbulence model constant		$C_{2\varepsilon}$	1.92
k-ε turbulence model constant		C_μ	0.09
k-ε turbulence model constant		σ_k	1
k-ε turbulence model constant		σ_ε	1.3

Table 2 shows that when the length, width, and height of the computational domain were 14 times the length of the storage pile (6 times forward and 7 times backward), twice the width of the pile, and seven times the height of the pile, the surface shear stress, a macroscopic variable of the storage pile, remained nearly constant. Therefore, Model 7 was determined to be the optimal computational domain (14 L × 2 W × 7 H), and thus the mutual restriction between the computation accuracy and calculation amount—the dilemma in the selection of calculation area—was resolved.

Mesh and Turbulence Model Definitions

Turbulence models used to simulate the airflow around porous fences are divided into standard k-ε turbulence models, and realizable k-ε turbulence models. These two models were used to calculate the $U/U_{0.4}$ at fixed heights of z = 0.38 h and z = 1.88 h; the results are compared in Fig. 2. The standard k-ε turbulence model at z = 0.38 h exhibited a more satisfactory fit to the experimental data than the realizable k-ε turbulence model did; however, the realizable

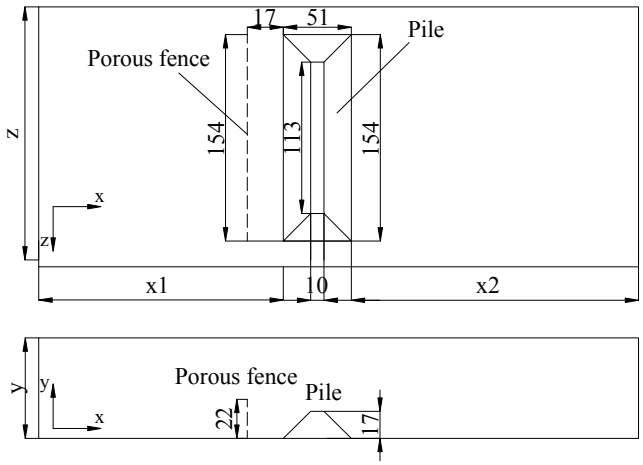

Fig. 1. Computational domain and boundary conditions.

Table 2. Physical dimension of computational domain and the shear stress on flat-top surface.

Model	x1 (m)	x2 (m)	Y (m)	Z (m)	The shear stress on flat-top surface (N)
1	153	255	85	308	259.2
2	153	357	85	308	250.3
3	204	357	85	308	248.3
4	255	357	85	308	240.2
5	306	357	85	308	246.9
6	306	357	102	308	234.1
7	306	357	119	308	234.0

Table 3. Boundary conditions for numerical simulation.

Computational boundary	Boundary conditions
Inflow surface	Velocity-inlet
Outflow surface	Outflow
Upper of computational domain	Symmetry
Lateral of computational domain	Symmetry
Floor	Wall
Flat-top surface of storage pile	Wall
Windward side of storage pile	Wall
Lee side of storage pile	Wall
Fence	Porous-jump

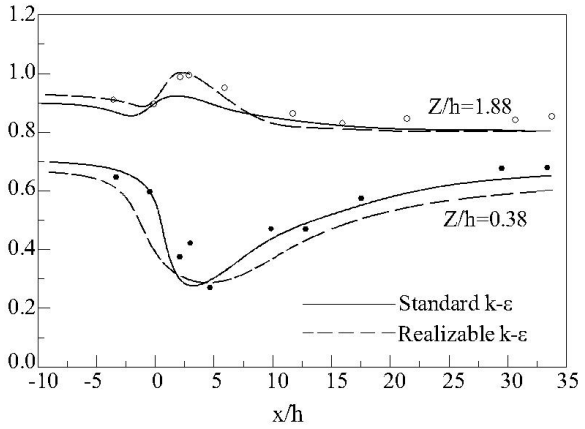

Fig. 2. Comparison of normalized predicted and experimental air velocities for the porous fence.

k-ε turbulence model exhibited more satisfactory results at z = 1.88 h. Because the airflow structure in the shear layer (z ≤ 0.77 h) was closer to z = 0.38 h than to z = 1.88 h, the standard *k-ε* turbulence model was used to simulate the air field.

The unstructured grids were generated in the computational domain; the whole area contained 1,755,883 grid nodes after the grid independence test was conducted. A second-order upwind scheme was used to discretize higher-order convection terms. The SIMPLE algorithm was selected, and the convergence criteria were set at 0.00001.

RESULTS AND DISCUSSION

Airflow Fields

The standard *k-ε* turbulence model was used to calculate airflow fields over the prismatic pile in unfenced conditions; the results are shown in Fig. 3. Incoming air (5 m/s) was determined to flow around the material stack, obstructing the natural air pattern and decreasing the airway area. Because of the windward slope, air velocity gradually increased and reached the maximum value of 8.32 m/s at the top of the slope. The wind shear also gradually increased from the bottom of the slope to the top. The flow velocity on the boundary layer (6.3 m/s), occurring at a height of 20 mm above the flat-top surface of the pile, accelerated to a speed greater than the incoming air speed. Velocity vector fields showed that the downwind pile had lower wind speeds resulting from increased airflow in the cross-sectional area, and that air pressure increased along the leeward slope, inducing a vortex and circumfluence in the downstream, and allowing particles to be emitted from the piles.

Airflow structure behind porous fences are determined by interaction between bleed flow passing through the holes of the fences and displaced flow passing over the fences, the ratio between the quantities of bleed air and displaced air differs as the fence porosity changes. Fig. 4 shows the velocity vector fields around the fence with various values of ε and their respective prismatic models. When the porous fence was set in front of the pile at a distance equal to the height of the material stack, and a porosity of 0 (a solid fence), the porous fence blocked incoming air; airflows over the top of the windbreak reached a maximum velocity of 6.61 m/s. Because of the vertical air pressure difference in the region between the windbreak and windward side, a vortex with a center higher than the top of the pile was induced. The air thus flowed downward along the windward slope, blowing material particles to the ground, or sweeping them up. Moreover, when the porosity was 0.2, a recirculating flow in the region between the fence and the pile emerged, and the resulting intensity of the vortex and the vortex diameter were smaller than when the porosity was 0. This is because bleed flow passing through the fence holes was far less than the airflow over the fence. The velocity gradually increased from the foot of the windward slope, reaching a maximum velocity of 6.004 m/s at a height of 10–11 m, and decreasing with increasing height as the shear force acted downward along the slope surface. Unlike in

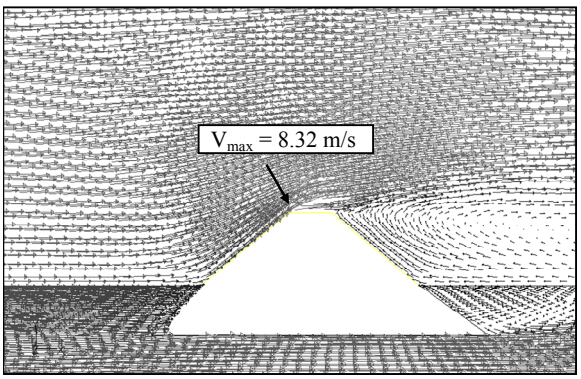

Fig. 3. Velocity vector fields over the prismatic pile without fence.

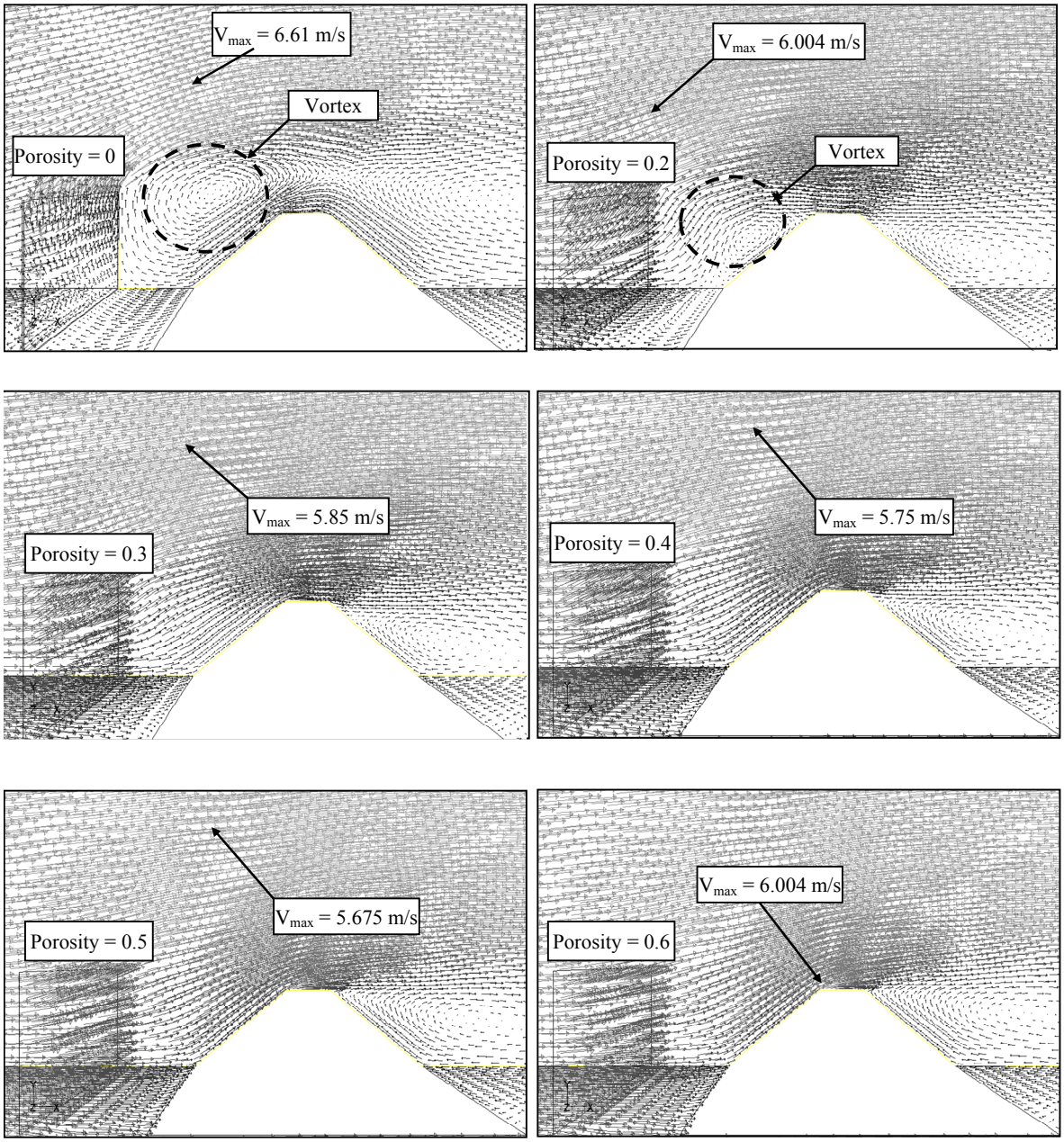

Fig. 4. Velocity vector fields over the prismatic pile behind fence.

unfenced conditions, the maximum velocity did not occur at the windward surface crest. When the porosities were 0.3, 0.4, 0.5, and 0.6, the approaching flow accelerated along the windward side of the pile, reaching maximum velocity at the top of the pile, where the shear force acted upward. The wind speed immediately above the prismatic pile exhibited a lower velocity than without the porous fence. This indicated that smaller porosity induced decreased flow velocity.

Flow fluctuation, therefore, is a function of the porosity (ε) of the fence. The turbulence characteristics of flow fields around fences of small porosity (ε = 0, 0.2) considerably differed from those around fences of large porosity (ε = 0.3, 0.4, 0.5, 0.6). Fences with porosity ε = 0.3, 0.4, 0.5, and 0.6, all decreased air velocity and shear force on the pile surfaces, reducing dust emissions. As in unfenced conditions, maximal dusting occurred on the top of the windward side of the pile. However, fences of porosities 0 and 0.2 altered the flow field characteristics around the pile. A recirculating flow in the region between the fence and the pile emerged, and approaching air flowed down the windward side instead of accelerating up. Dust slid down the windward surface to the ground, or was blown against the fence; maximal dusting did not occur at the crest, but rather at the center of a vortex two-thirds the height of the windward slope.

The mean velocity profiles in oncoming wind direction are shown in Fig. 5. We put emphasis on wind speed variation tendencies at various heights surrounding the material pile. At a height of 18 m, 1 m higher than the top of the pile, the flow decelerated sharply through the porous fence (x = –42.5 m) and the shear velocity of the top of the

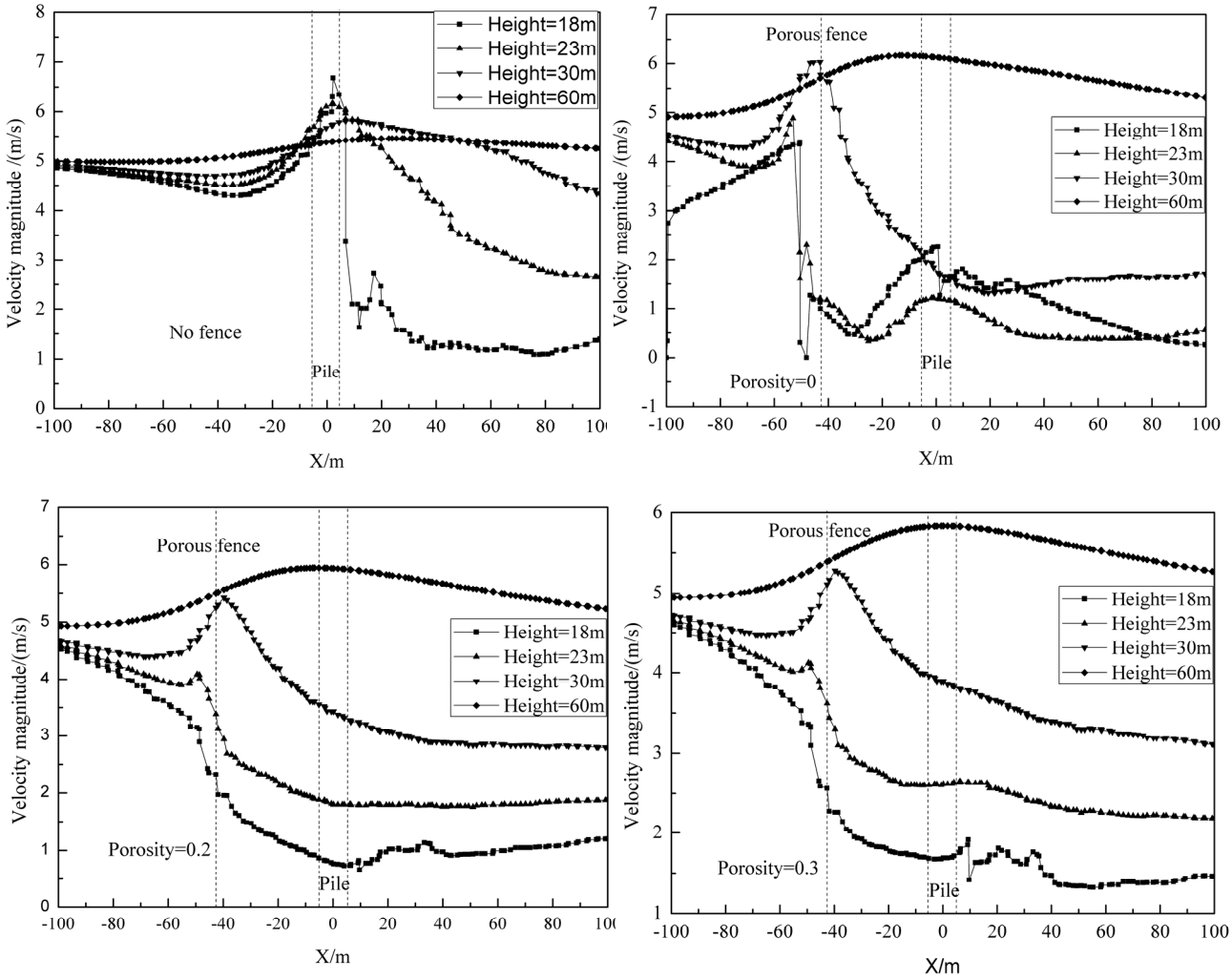

Fig. 5. Velocity magnitude diagram at different altitude.

material stack (x = –5–5 m) substantially declined. At a height of 23 m, 1 m higher than the top of the pile, when airflow approached the fence, the airflow velocity increased to different extents. The results showed that there was a great difference in the streamline lifting with different porosity, as the porosity increased, the airflow velocity increased slowly. A low-velocity region formed behind the fence due to the wind's momentum transferred. At a height of 30 m, the displaced flow that passes over the fences took the dominant position, the flow accelerated rapidly over the porous fence, then decelerated gently behind the fence. At a height of 60 m, and the airflow velocity changed gradually; subsequent increases in velocity occurred only at the upwind and top surface sections.

Surface Shear Stress Distribution

Dust emissions from material piles are closely related to forces applied on the pile surfaces. Although the suffering force characteristics of particles in stacked material are complicated, shear stress in the thin layer of air near the pile surface contributes substantially to dust emissions. Consequently, this study focused on the distribution of shear stress on pile surfaces to investigate the sheltering effect of porous fences. The analysis indicated that fence porosity exerted a substantial effect on airflow distribution and pressure loss behind porous fences; that shear stress acted on the windward side; and that the windward side, flat-top, and leeward side all exhibited unique characteristics. Analyzing and predicting stress on each surface is crucial to determining the optimal porosity of a porous fence. Fig. 6 shows the distribution of shear force on each prismatic surface as a function of fence porosity, and clearly illustrates the differences in dust emissions from the three surfaces. The simulation results revealed that the windward surface experienced the greatest shear force, followed by the flat-top, and then the leeward surfaces.

Shear force on the windward surface acted upward with a value of 325.6801 N in unfenced conditions. The existence of a porous fence, not unexpectedly, changed the original airflow around the piles. When the porosity was 0.3–0.6, the volume of air passing through the fence decreased, and both air pressure and velocity behind the fence also decreased. The surface shear force in the thin boundary layer was reduced, thus decreasing the amount of dust emitted. In general, however, the shear stress was positive and the surface shear effect acted upward along the windward face.

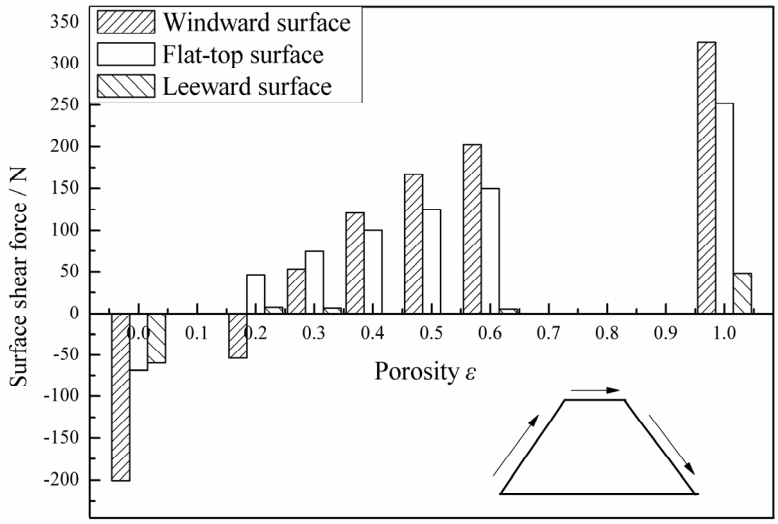

Fig. 6. Shear force on the pile surfaces behind porous fence with deferent porosity.

With an increase in porosity, the shear stress on the windward surface of the pile increased gradually. When the porosity was 0.3, the shearing force was 52.96956 N, or 16.26% of the shearing force in unfenced conditions. When the porosity was 0 (a solid fence) and 0.2, the shear stress was negative; in other words, the surface shearing action occurred downward along the windward face. This is because at small porosities, the volume of seepage air through the fence holes was small, the sharp drop in wind pressure behind the fence induced a vertical differential pressure increase, and high pressure air in the upper part flowed downward, forming a vortex flow above the windward surface. Surface shear force for a fence with a porosity of $\varepsilon = 0$ was as high as 200.736 N downward; this was nearly the same absolute value as that for a fence with a porosity of 0.6 and much greater than that for a fence with a porosity $\varepsilon = 0.2$, which was only 53.8 N because the intensity of the vortex flow was stronger between the fence and the windward surface. Airflow pressure was reduced behind the fence with decreasing fence porosity, because of an increase in the quantity of air flowing over the fence and an increase in the air flowing through the fence holes. Thus, the amount of dust emitted from the windward surface was lowest when ε was 0.2 and 0.3. At porosities greater than 0.3, the porous fence reduced the airflow velocity around the surfaces of the pile, thereby also reducing the surface shear force. Reduced porosity also enhanced the sheltering effect: at porosities less than 0.3, air did not flow up the windward slope, but rather, formed a local eddy current, shifting the airflow downward, as well as the dust particles, which moved downward under the downward shear force. Simulation results showed that the optimal porosity should be between 0.2 and 0.3 above or below which the shear force characteristics on the windward surface differed strongly, and porosities of either 0 or 0.6 do not substantially reduce dust emissions.

In unfenced conditions, shear stress on the flat-top surface acted in the incoming airflow direction with a value of 325.6801 N. Airflow velocity decreased behind the fence, wind in the thin boundary layer above the flat-top slowed, and the shear surface force decreased. At a porosity of 0.2, the shearing force on the top of the pile was 46.2023 N, or 18.34% of that in unfenced conditions. At a porosity of $\varepsilon = 0$, the shear stress was negative, and much greater than that of $\varepsilon = 0.2$. The high vortex intensity behind the solid fence rendered the top surface a continual backflow region, and air in the thin upper layer, flowing against oncoming airflows, caused the emission of material particles to be reversed. Fig. 6 showed shear stress on the flat-top surface increased with increasing porosity when the porosity is greater than 0.2. Taken together, shear force on the top surface decreased firstly and then increased with increasing porosity, the lowest value is at the porosity of 0.2; consequently, the amount of dust from the top surface was the lowest when $\varepsilon = 0.2$.

Because the leeward side is always in the backflow region, the shear stress on the leeside was considerably lower than on the windward and flat-top surfaces. The maximum shear force was only 47.90497 N in unfenced conditions. Therefore, particles are mainly raised from the windward slope and flat-top surfaces. As shown in Fig. 6, the surface shear force for a fence with a porosity of $\varepsilon = 0$ was as high as 59 N upward, with an absolute value a little larger than in unfenced conditions; this is because at $\varepsilon = 0$, air pressure fell sharply after flowing around the windbreak, all of the surfaces of the stock pile were in negative air pressure zones and, as a result, dust particles were lifted up from leeward surface under the effect of the vortex flow. Shear stress was comparatively reduced for fences with porosities $\varepsilon = 0.2$–0.6, and exhibited little change with increasing ε between 0.2 and 0.6. Material particles were lifted up along the leeward slope and then down, under the action of the airflow near the thin boundary layer. This indicated that a porous fence with a small porosity, such as 0.2 or 0.3, exhibited a greater sheltering effect.

The analysis revealed that fence porosity is an important parameter that affects airflow field characteristics and aerodynamic structures around storage piles. Based on the flow field data, a porous fence with a porosity of 0.2–0.3 is optimal.

CONCLUSIONS

Using CFD, this study investigated airflow structure and dust emissions behind porous fences used to shelter open storage piles.

The prediction results revealed that the placement of a porous fence, in relation to an open storage pile, impacted the aerodynamic structure of the surrounding airflow fields. A highly turbulent flow fields was formed by the interaction between bleed flow passing through the holes of the fences and displaced flow passing over the fences. Porosity played a crucial role in the forming of leeward velocity field. At small porosities ($\varepsilon = 0, 0.2$), airflow did not accelerate up along the windward side, but rather, a recirculating flow in the region between the fence and the pile emerged. Maximum dust emission did not occur on the top, as is the case in unfenced conditions, but rather at two-thirds the height of the windward side.

By analyzing the shear force distribution on the pile surfaces, we revealed an internal relationship between the fence's porosity and the surface shear stress characteristics. The results indicated that the effect of shear stress varies among the various surfaces. The shear stress acts downward along the windward slope for fences of porosity $\varepsilon = 0$ and 0.2, and the value of the shear stress at porosity $\varepsilon = 0.2$ was substantially less than at porosity $\varepsilon = 0$. At porosities greater than 0.3, the shear force acted upward along the windward side, and increased with increasing porosity. Shear force on the flat-top surface first decreased, then increased with increasing porosity, and the least amount of shear force occurred at a porosity of $\varepsilon = 0.2$. Fences of porosities $\varepsilon = 0.2$–0.6 greatly reduced the value of the shear stress on the prismatic leeside, and exhibited little change with increasing ε between 0.2 and 0.6.

In this study, a porous fence with different porosities ($\varepsilon = 0$, 0.2, 0.3, 0.4, 0.5, and 0.6) to shelter a storage pile in an open storage yard was simulated. The optimal values for reducing dust emission were $\varepsilon = 0.2$ and 0.3.

We employed CFD to obtain precise velocity fields behind porous fence to provide a deeper understanding of the optimal porosity. This result relates the optimal fence porosity to the distribution of shear stress on pile surfaces. Further studies will focus on the relationship between the other parameters such as turbulence and pressure of optimal fence porosity.

ACKNOWLEDGMENTS

This study was financially supported by the Natural Science Foundation of China (NSFC), under grants 51108295 and 41173002.

REFERENCES

Badr, T. and Harion, J.L. (2005). Numerical Modelling of Flow over Stockpiles: Implications on Dust Emissions. *Atmos. Environ.* 39: 5576–5584.

Badr, T. and Harion, J.L. (2007). Effect of Aggregate Storage Piles Configuration on Dust Emissions. *Atmos. Environ.* 41: 360–368.

Bitog, J.P., Lee, I.B. and Shin, M.H. (2009). Numerical Simulation of an Array of Fences in Saemangeum Reclaimed Land. *Atmos. Environ.*43: 4612–4621.

Chen, G.H., Wang, W.W., Sun, C.F. and Li, J.L. (2012). 3D Numerical Simulation of Wind Flow Behind a New Porous Fence. *Powder Technol.* 230: 118–126.

Cong, X.C., Yang, S.L. and Cao, S.Q. (2012). Effect of Aggregate Stockpile Configuration and Layout on Dust Emissions in an Open Yard. *Appl. Math. Modell.* 36: 5482–5491.

Diego, I., Pelegy, A., Torno, S., Torano, J. and Menendez, M. (2009). Simultaneous CFD Evaluation of Wind Flow and Dust Emission in Open Storage Piles. *Appl. Math. Modell.* 33: 3197–3207.

Dong, Z.B., Luo, W.Y., Qian, G.Q. and Wang, H.T. (2007). A Wind Tunnel Simulation of the Mean Velocity Fields behind Upright Porous Fences. *Agric. For. Meteorol.* 74: 193–207.

Dong, Z.B., Luo, W.Y., Qian, G.Q., Lu, P. and Wang, H.T. (2010). A Wind Tunnel Simulation of the Turbulence Fields behind Upright Porous Wind Fences. *J. Arid. Environ.* 74: 193–207.

Gillette, D. (1978). A Wind Tunnel Simulation of the Erosion of Soil: Effect of Soil Texture, Sandblasting, Wind Speed, and Soil Consolidation on Dust Production. *Atmos. Environ.* 12: 1735–1743.

Guo, L. and Maghirang, R.G. (2012). Numerical Simulation of Airflow and Particle Collection by Vegetative Barriers. *Eng. Appl. Comput. Fluid Mech.* 6: 110–112.

Heisler, G.M. and Dewalle, D.R. (1988). Effects of Windbreak Structure on Wind Flow. *Agric. Ecosyst. Environ.* 22: 41–69.

Kim, H.C., Lee, C.M. and Lim, H.C. (1997). An Experimental and Numerical Study on the Flow over Two-dimensional Hills. *J. Wind Eng. Ind. Aerodyn.* 66: 17–33.

Lee, S.J. and Kim, H.B. (1999). Laboratory Measurements of Velocity and Turbulence Field behind Porous Fences. *J. Wind Eng. Ind. Aerodyn.* 80: 311–326.

Lee, S.J. and Lim, H.C. (2001). A Numerical Study on Flow around a Triangular Prism Located behind a Porous Fence. *Fluid Dyn. Res.* 28:209–221.

Mao, Y., Wilson, J.D. and Kort, J. (2013). Effects of a Shelterbelt on Road Dust Dispersion. *Atmos. Environ.* 79: 590–598.

Parsons, D., Wiggs, G., Walker, I. and Ferguson, R. (2004). Numerical Modelling of Flow Structure over an Idealized Transverse Aeolian Dunes of Varying Geometry. *Geomorphology* 59: 149–164.

Parsons, D., Wiggs, G., Walker, I., Ferguson, R. and Garvey, B. (2004). Numerical Modelling of Airflow over an Idealized Transverse Dune. *Environ. Modell. Softw.* 19: 153–162.

Raupach, M.R., Woods, N., Dorr,G., Leys, J.F. and Cleugh, H.A. (2001). The Entrapment of Particles by Windbreaks. *Atmos. Environ.*35:3373–3383.

Rosenfeld, M., Marom, G. and Bitan, A. (2010). Numerical Simulation of the Airflow across Trees in a

Windbreak. *Boundary Layer Meteorol.* 135: 89–107.

Torano, J.A., Rodriguez, R., Diego, I., Rivas, J.M. and Pelegry, A. (2006). Influencee of Pile Shape on Wind Erosion CFD Emission Simulation. *Appl. Math. Modell.* 31: 2487–2510.

Turpin, C. and Harion, J.L. (2009). Numerical Modeling of Flow Structures over Various Flat-topped Stockpiles Height: Implications on Dust Emissions. *Atmos. Environ.* 43:5579–5587.

White, B. and Tsoar, H. (1998). Slope Effect on Saltation over a Climbing Sand Dune. *Geomorphology* 22: 159–180.

Xuan, J. and Robins, A. (1994). The Effect of Turbulence and Complex Terrain on Dust Emissions and Depositions from Coal Stock Piles. *Atmos. Environ.* 28: 1951–1960.

Yeh, C.P., Tsai, C.H. and Yang, R.J. (2010). An Investigation into the Sheltering Performance of Porous Windbreaks under Various Wind Directions. *J. Wind Eng. Ind. Aerodyn.* 98: 520–532.

Zhang, Z.D., Wieland, R. and Reiche, M. (2011). Wind Modelling for Wind Erosion Research by Open Source Computational Fluid Dynamics. *Ecol. Inform.* 6: 316–324.

Received for review, December 16, 2013
Accepted, February 14, 2014